

RESEARCH

Open Access



# Determination of maximum additional load for EV charging station considering practical security limits

Sayak Mondal<sup>1\*</sup> , Parimal Acharjee<sup>1</sup> and Aniruddha Bhattacharya<sup>1</sup>

\*Correspondence:  
Sm.21ee1106@phd.nitdgp.ac.in

<sup>1</sup> Department of Electrical Engineering, National Institute of Technology, Durgapur, West Bengal 713209, India

## Abstract

Nowadays, the allocation of electric vehicle charging stations (EVCS) for the charging of electric vehicles (EVs) is essential, as random allocation may cause significant energy loss for the radial distribution system (RDS). Uncoordinated charging of EVs dominates the load profile of the RDS. Although a single EV has a negligible impact on the system, the combined effect of charging an EV cluster may violate the voltage security constraints of the RDS. Therefore, to avoid such circumstances, the loadability limit of each node of the RDS must be determined. Previously, conventional analytical methods were used to calculate the maximum loadability of the RDS node, where voltage magnitudes become less than the critical voltage limit. However, these approaches are not acceptable for the power industry, as it may push the system towards a blackout. Therefore, the appropriate capacity of the EVCS can only be determined if the voltage security limit of each node of the RDS follows its critical limit. Hence, in this paper, a modified forward-backward sweep (MFBS) algorithm is formulated to find the maximum additional load (MAL) of each node of the RDS considering non-unity power factor during the EV charging process. This algorithm may help the EVCS to determine its capacity or optimal number of charging ports directly during installation at an optimal location of RDS. For validation, the 33-bus and 69-bus RDSs have been used, and it can be seen that the EVCSs have been successfully installed in the optimal location of the test systems mentioned above without violating the voltage security limit of each node of the RDS.

**Keywords:** Forward-backward sweep method, Maximum additional load, EV charging station, Security limits

## Introduction

The modern power system is tending towards the zero-carbon emission. On the other hand, global warming is an alarming issue for the whole world. Basically, based on these two factors, slowly the Electric Vehicle (EV) is grabbing attention in the society by replacing internal combustion engine (ICE) vehicles [1, 2]. As day by day, the efficiency and the performances of EVs are being improved, EVs are the most convenient transportation in future [2]. The use of EVs has increased mainly due to the pollution free environment and lower fuel cost. But charging of EVs as well as suitable EV Charging

station (EVCS) is the prime concern for the use of EVs because EV charging during travelling is required [3, 4]. In this regard, it is important to determine the optimum capacity of EVCS for each bus. If for each bus, the maximum permissible extra load for which the operation of power system network will be safe and secure is known, the optimum capacity of the EVCS can be assessed. In this paper, formula-based approach is proposed to determine the maximum additional load ( $MAL$ ) for each bus.

The development of a widespread charging infrastructure is essential for charging EVs and developed countries have already been planned to install EVCS in order to encourage the use of EVs [5, 6]. In order to achieve the 7 million public and private chargers in France by 2030, 2 billion Euros will be needed to upgrade the public and residential charging infrastructure in major U.S. metro areas [7]. Since EV charging infrastructure needs to be installed, existing distribution networks must be upgraded, formal methods of locating and sizing EV chargers must be researched based on the demand scenario and voltage limit of existing distribution grids [8]. The presence of EV chargers in distribution grids can result in a congested transformer in the substation, a voltage violation, and a loss of power for the distribution system [9]. Furthermore, the RDS can experience voltage collapse if, at some point, many EVs charge in an uncontrollable way in one node. To avoid voltage violation of the RDS, the suitable rating of EVCS should be evaluated. If the rating of EVCS is known, the appropriate number of charging ports that can parallel run can also be determined easily.

To determine the loadability limit or load margin or voltage stability index (VSI), different approaches were proposed in the available literature [10–17]. In [10], the voltage stability index (VSI) was determined based on Jacobian matrix of load flow. In these studies, Jacobian matrix was modified and Eigen values were used for the determination of VSI. Here, the variations in voltage and reactive power were highlighted, but it is more important to emphasise on the active power consideration during EV charging applications, not been addressed comprehensively in the above mentioned literatures. Again, using a multi-objective optimization technique, a solution of bus loadability limit was evaluated considering both active and reactive power margin [11]. In [11], both PV and QV curve were considered. The maximum loadability limit was determined to obtain the maximum load margin or the voltage collapse point. But practically, the maximum load cannot be applied for safety and secure operation of the power system because the voltage magnitude will be below the lower voltage limit. Therefore, voltage deviation is not analysed in this work. In [12], to identify the most vulnerable bus in the power system network, L-index and voltage collapse proximity index (VCPI) were applied in order to avoid potential outages and blackouts. When a wind farm is integrated to a distribution system, its VSI or loadability limit will change because of the practical operating constraints of the distribution system [13]. Considering this real time safety operation, a new VSI was developed in [13]. In [12, 13], the voltage which is obtained that is near about the unstable operating point. That is not desirable for the safe operation of the power system. In [14], a unique approach based on the machine learning was proposed to predict the long-term voltage stability, which was represented by an intuitive and simple indicator namely loadability margin (LM). The proposed method used different VSIs to obtain long-term voltage stability [14]. In [15], a new line voltage stability index was proposed to identify weak lines and buses for a variety of loading scenarios and network

topologies. In [14, 15], VSI index is applied to analysis only one node of the RDS. If load is increased for a bus, the voltage magnitudes of all load buses are reduced. But, the voltage at all nodes were not analysed in this work. In [16], Yue Song et al. proved that the Jacobian matrix of load flow becomes singular when the network load admittance ratio is unity. Based on this concept, a new VSI was proposed, that was linear with load increment under different test scenarios. The proposed VSI can also provide the impact of DG integration [16]. But in [16], it is only considered that DGs can only deliver the active power whereas DGs may deliver both active and reactive power. But here, the reactive power factor has not been considered. A new voltage recovery index (VRI) was developed to judge the overall system strength for the incorporation of renewable energy generation [17]. At the system level, it also helps to quantify the short-term voltage stability (STVS). In this index, only active power load was taken into account but reactive power load was not considered [17], which is very much essential for the EV charging process.

Considering these literatures along with its limitation, the scope of work is identified as (i) the authors must consider both active and reactive power together for doing the analysis related to the EV charging applications. (ii) As the voltage security limit is not analysed properly to find the loadability limit of each nodes of a RDS, the maximum loadability limit of a node should be determined in such a way that all the bus voltages of RDS must remain above the critical voltage limit. (iii) There should be a new modified index, which will not allow the system to go beyond the threshold of voltage limits.

As the charging of an EV with optimum capacity is a challenging task, hence it is very important to identify the extra load of a node for which voltage magnitude of any node of that system should not be less than the critical voltage ( $V_{cri}$ ) for the safe and secure operation of the power system. If the load increases for a node of a RDS, the voltage magnitude reduces not only for that particular node, but voltage magnitudes of other nodes are also decreased [18, 19]. Hence,  $MAL$  of each node for a RDS is required to determine considering the practical security constraint, i.e., upper and lower voltage limits. For this purpose, first the load flow analysis of a RDS system is required and then extra allowable load for which the node voltage of the RDS should not be less than the lower voltage limit should be determined.

Fundamentally, one of the most widely used methods for distribution system load flow analysis is the FBS (forward-backward sweep) approach. As the FBS method follows the simple and basic KCL and KVL theory, the method is very simple, and its execution is also easy. From the literature survey [7, 20], it can be clinched that EV mainly consumes more active power and very less reactive power. Based on this hypothesis, the power factor of the bus where EVCS will be connected is set to  $pf$ . Active power is first computed, and once that has been updated, reactive power is then assessed in order to keep the power factor at  $pf$ . Considering this, the modified FBS is developed to determine the  $MAL$  of that bus so that all bus voltage of the network should be more or equal to  $V_{cri}$  p.u., critical voltage. The developed modified FBS is examined on the 33-bus and 69-bus RDS.

The primary contributions of this paper are as follows:

- To overcome the research gaps, in the proposed algorithm, both active and reactive power are considered for EV charging process by connecting it with RDS. The battery

of EV consumes mainly active power and the charging circuit consumes little amount of reactive power [7]. Based on this philosophy, the power factor of the node should be considered where EVCS to be placed.

- As the voltage security constraints are not analysed properly to find the loadability limit of each nodes of a RDS, a maximum additional load (*MAL*) of a node is determined by maintaining the voltage within the acceptable limit of all the nodes of RDS. The percentage of voltage deviation that is considered acceptable for RDS falls anywhere between 10% and  $-10\%$ . If the voltage deviation exceeds these limits, then the system may go to the point of voltage instability and connected loads will not be able to operate properly. Hence, checking the voltage security limits for all the buses is essential after performing the load enhancement.
- *MAL* is determined in order to maintain the voltage range at a level that is higher than the critical voltage security limit. When the *MAL* is determined for a specific bus, it is easier to determine the number of electric vehicles' batteries that can be connected with RDS and charged simultaneously without violating the voltage security constraints.

The paper is represented as follows: in [Methods](#) section basics of forward backward sweep method is described; problem statement is highlighted, proposed MFBS algorithm is discussed and flowchart of complete algorithm is shown; in [Results and discussion](#) section, results and discussion is given with some case studies; in [Conclusions](#) section, conclusion of that paper is conferred.

## Methods

### Existing methods

#### *Forward-backward sweep (FBS) method*

Basically, the FBS method is one of most popular method for load flow analysis of distribution system because R/X ratio is high in radial distribution system and this method is very easy to handle. Generally, distribution system is considered to be weakly meshed and radial type [21]. Based on the analysis as shown in [21], it can be revealed that forward-backward sweep (FBS) method is one of the most promising and efficient methods for load flow analysis in radial distribution system (RDS). FBS technique is basically based on the theory of Kirchhoff's voltage law (KVL) and Kirchhoff's current law (KCL). This method requires backward sweep for branch current calculation and forward sweep for determining the voltage.

In forward-backward sweep (FBS) method, two dissimilar approaches are available. First one is based on the power flow [22–25] and another is on the current flow [21, 26–29]. Power flow in each system branch, power injected by each generating source, voltage magnitude and phase angle at each system bus, and system losses are all determined using load flow (LF) analysis. The distribution system's power flow formulation might be either single-phase or three-phase.

### Proposed method

#### *Problem statement*

In general, load enhancement is determined keeping the power factor constant. In other words, the ratio of active and reactive power will remain same when dealing with any

other type of non-elastic load besides electric vehicles (EV). But EVs consume a little amount of reactive power and consume more active power. As a result, power factor will be little high. From the literature survey [7], the power factor will be improved to approximately  $pf$  when EV load will be connected to that particular node.

Using FBS method first the additional extra active power ( $MAL$ ) is calculated. Using Eq. (1) the modified/ updated active power ( $P_{mod}$ ) is calculated. After that, updated/modified reactive power ( $Q_{mod}$ ) will be determined using (4) keeping the power factor  $pf$ .

$$P_{mod} = (P_{Li} + MAL) \quad (1)$$

According to the problem statement, the power factor =  $pf$

Hence,  $\cos\phi = pf$

$$\begin{aligned} \text{or, } \phi &= \cos^{-1}(pf) \\ \text{or, } \tan\phi &= \tan(\cos^{-1}(pf)) \end{aligned} \quad (2)$$

Let, the modified active power load =  $P_{mod}$  and the modified reactive power load =  $Q_{mod}$

Now,

$$\begin{aligned} P_{mod} &= (P_{Li} + MAL) \\ \frac{Q_{mod}}{P_{mod}} &= \tan\phi \\ \text{or, } Q_{mod} &= P_{mod} * \tan\phi \end{aligned} \quad (3)$$

From (2) and (3), we get,

$$\begin{aligned} Q_{mod} &= (P_{Li} + MAL) * \tan(\cos^{-1}(pf)) \\ \text{or, } Q_{mod} &= P_{Li} * \tan(\cos^{-1}(pf)) + (MAL * \tan(\cos^{-1}(pf))) \\ \text{or, } Q_{mod} &= (Q_{Li} + (MAL * \tan(\cos^{-1}(pf)))) \end{aligned} \quad (4)$$

Here,  $Q_{Li} = P_{Li} * \tan\phi$

Where,  $P_{Li}$  and  $Q_{Li}$  indicate the real and reactive load power at node  $i$  respectively.

In Fig. 1, the bus 1 can be termed as substation bus whose voltage is assumed to be complex. Corollary, the substation bus can be termed as root node for the LF purpose and the end nodes of each branch can be termed as the leaf node.  $MAL$  is the maximum additional load apart from the connected base load at  $m$ th node and  $(m-1)$  is the node of the previous node of the  $m$ th node. The node which is having least voltage after incorporation of  $MAL$  at node  $m$ , is assumed to be  $V_{cri}$ . The value of voltage to be maintained as  $V_{cri}$ , is decided by the utility. Accordingly, the value of  $MAL$  of  $m$ th node is calculated which can maintain lowest voltage of the network at  $V_{cri}$ .

#### **Steps of proposed modified forward backward sweep method**

Like FBS method, flat start is initialized, and the root node is taken as the reference node for the proposed MFBS method. To find the maximum allowable extra load for a node, a new additional factor  $MAL$  is added for increasing the load to a node in the MFBS load flow method. In this iterative process,  $MAL$  is providing the threshold value of additional load. Based on this concept and objective, to evaluate  $MAL$ , some modifications have been proposed and described step-wise:

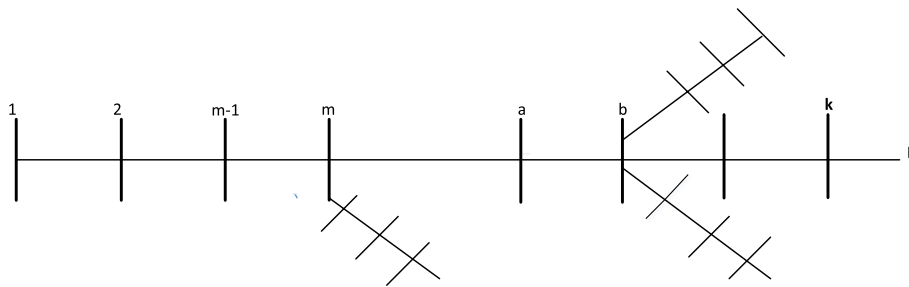


**Fig. 1** A radial distribution system

Step 1: Initialize the unknown voltage magnitude and phase angle as flat start.

Step 2: Initialization of iteration count  $t=0$

Step 3: The apparent power and node voltage are therefore used to calculate the current at each bus. At iteration  $t$ , load current  $I_i^t$  at node  $i$  is calculated as

$$I_i^t = \left[ \frac{P_{Li} + jQ_{Li}}{V_i^{t-1}} \right]^* ; \text{ for } i = 2, 3, \dots, (N - 1) \dots \text{ (Except } m - \text{ node)} \quad (5)$$

In (5),  $P_{Li}$  and  $Q_{Li}$  indicate the real and reactive load power at bus  $i$  respectively, while  $V_i^{t-1}$  indicates the complex bus voltage of bus  $i$  corresponding to  $t-1$ th iteration.

Step 4: If a load is connected by adding a factor of  $MAL$  with the consideration of a power factor ( $pf$ ) at  $m^{th}$  node of RDS, then the modified load current ( $I_m^{CP}$ ) of that particular node is evaluated as:

$$I_m^{CP} = \left[ \frac{(P_{Li} + MAL) + j(Q_{Li} + (MAL * \tan(\cos^{-1} pf)))}{V_m^{t-1}} \right]^* \quad (6)$$

Where  $MAL$  denotes the Maximum Additional Load at the  $m$ th node and  $V_m^{t-1}$  is the voltage of  $(m-1)$  at  $(t-1)$ th iteration. It checks the maximum loadability limit of that particular node for maintaining the critical voltage level.

Step 5: In modified backward sweep, basically the branch current calculation is started from the end leaf node and moving towards the root node. For example, in Fig. 1, the current in the branch between the buses  $a$  and  $b$  at iteration  $t$  ( $I_{ab}^t$ ) is given by:

$$I_{ab}^t = I_b^t + \sum I_{sum} \quad (7)$$

In (7),  $I_{ab}$  denotes the current flowing through branch  $a-b$ ,  $I_b$  denotes the individual load current of node  $b$  and  $I_{sum}$  indicates the summation of all current of branches emanated from node  $b$ .

After integrating  $MAL$  at  $m^{th}$  node, the branch currents are also modified as

$$I_{(m-1),m}^t = I_m^{CP} + \sum I_{sum(mod)} \quad (8)$$

By putting the value of  $I_m^{CP}$  from Eq. (6) in Eq. (8):

$$or, I_{(m-1),m}^t = \left[ \frac{(P_{Li} + MAL) + j(Q_{Li} + (MAL * \tan(\cos^{-1} pf)))}{V_m^{t-1}} \right]^* + \sum I_{sum(mod)} \tag{9}$$

In (9),  $I_{(m-1),m}$  indicates the current flowing through branch (m-1)-m and  $I_{sum(mod)}$  is the modified summation of all current of branches emanated from node m.

Step 6: In modified forward sweep, the voltages at each node are updated from the root node to the leaf node with respect to the voltage at the respective trailing node. In Fig. 1, the value of  $V_b^t$  is calculated as

$$V_b^t = V_a^t - Z_{ab} I_{ab}^t, \text{ for all } i = 2, 3, \dots, (N - 1) \text{ (except } m - \text{ node)} \tag{10}$$

In (10),  $V_a$  &  $V_b$  is the voltage of node a and b respectively,  $Z_{ab}$  denotes the impedance of branch a-b.

Now, considering the effect of MAL,  $m^{th}$  node voltage  $V_m$  is calculated as:

$$V_m^t = V_{m-1}^t - I_{m-1,m}^t * Z_{m-1,m} \tag{11}$$

After putting  $I_{m-1,m}^t$  in (11), the equation is written as:

$$\begin{aligned}
 or, V_m^t &= V_{m-1}^t - \left[ \left[ \frac{(P_{Li} + MAL) + j(Q_{Li} + (MAL * \tan(\cos^{-1} pf)))}{V_m^{t-1}} \right]^* + \sum I_{sum(mod)} \right] * Z_{m-1,m} \\
 or, (P_{Li} + MAL) - j(Q_{Li} + (MAL * \tan(\cos^{-1} pf))) &= \frac{((V_{m-1}^t - V_m^t) * V_m^{t-1})}{Z_{m-1,m}} - (\sum I_{sum(mod)} * V_m^{t-1}) \\
 or, MAL(1 - j \tan(\cos^{-1} pf)) &= \frac{((V_{m-1}^t - V_m^t) * V_m^{t-1})}{Z_{m-1,m}} - P_{Li} + jQ_{Li} - \sum I_{sum(mod)} * V_m^{t-1} \\
 or, MAL &= \frac{((V_{m-1}^t - V_m^t) * V_m^{t-1})}{Z_{m-1,m} * (1 - \tan(\cos^{-1} pf))} - \frac{(P_{Li} - jQ_{Li} + (\sum I_{sum(mod)} * V_m^{t-1}))}{(1 - \tan(\cos^{-1} pf))} \\
 or, MAL &= \frac{((V_{m-1}^t - V_m^t) * V_m^{t-1}) - (P_{Li} - jQ_{Li} + (\sum I_{sum(mod)} * V_m^{t-1})) * Z_{m-1,m}}{Z_{m-1,m} * (1 - \tan(\cos^{-1} pf))}
 \end{aligned} \tag{12}$$

In (11) and in (12),  $V_{m-1}^t$  denotes the voltage of (m - 1)-node at tth iteration,  $Z_{m-1,m}$  is the impedance between node (m - 1) and m.

The new and unique equations for MAL are formulated. To find out the value of MAL,  $V_m^t$  is replaced by the magnitude of  $V_{cri}$  in Eq. (12). So, MAL is derived as:

$$MAL = \frac{((V_{m-1}^t - V_{cri}) * V_m^{t-1}) - ((P_{Li} - jQ_{Li} + (\sum I_{sum(mod)} * V_m^{t-1})) * Z_{m-1,m})}{Z_{m-1,m} * (1 - \tan(\cos^{-1} pf))} \tag{13}$$

Step 7: Update current and voltage by putting the value of MAL in Eqs. (6), (9), and (11).

Step 8: Calculate

$$err_i^k = |V_i^t - V_i^{t-1}|, \text{ for all } i = 2, 3, \dots, N \tag{14}$$

Step 9: Calculate  $err_{max}^t = \max(err_2^t, err_3^t, err_4^t, \dots, err_N^t)$

$$err_{max}^t = \begin{cases} \text{Print the result; if } err_{max}^t \leq \text{tolerance value} \\ \text{Update the iteration count } t = t + 1, \text{ and go to step 3; otherwise} \end{cases} \tag{15}$$

In this algorithm, the critical node ( $k$ th node) is attached to a node which has the lowest voltage ( $V_{cri}$ ) compared to the other node voltage in RDS. Hence, in backward sweep, the sum of all currents is calculated towards this node. Correspondingly, in forward sweep, the voltage calculation starts from the  $MAL$  connected node ( $m$ -node). The  $MAL$  connected node concept is like connecting EV loads to RDS. Here,  $MAL$  is calculated based on the voltage magnitude of critical node. But in this algorithm the value of  $MAL$  is updated in every iteration and provides a final value after MFBS converged. Based on  $MAL$  into a node, the load of that node is modified and creates a ripple effect on the voltages of other nodes of the entire RDS system. The entire algorithm terminates when change in voltage is less than  $10^{-4}$ . By observing the value of  $MAL$ , an EVCS can understand the availability of charging port in a node and according to that it can decide how many EVs they allow to charge.

#### **Flowchart of the complete algorithm**

Following the calculation of  $MAL$  in (13), the system voltage of all the nodes is updated. Consequently, the update of system voltage will lead to updating the active power and reactive power at  $m$ -node in modified forward sweep. The entire problem has been solved in MATLAB 2022a version on a computer of AMD Ryzen 7. The procedures of the MFBS algorithm have been drawn in the flow chart of Fig. 2.

#### **Results and discussion**

The 33-bus and 69-bus RDS have been chosen for the validation of the proposed methodology. A single-line diagram of 33-bus RDS system, which has 33 buses and 4 lateral branches, is shown in Fig. 3 and 69-bus RDS system, which has 69 buses and 7 lateral branches, is shown in Fig. 4 [30, 31]. The total active power load is 3.72 MW and total reactive power load is 2.3MVAR for 33-bus system. Similarly, for 69-bus the active and reactive power is 3.8 MW and 2.69 MVAR, respectively. The base voltage is 12.66 kV and the base MVA is 100 MVA for both RDS.

The execution of the algorithm has been implemented on MATLAB software package. Using the proposed modified FBS method, the  $MAL$  is calculated for all the buses. But generally, the node which has the higher  $MAL$ , has been considered for EVCS placement. Hence, only eight nodes with higher value of  $MAL$  are represented. Both base active and reactive load are represented in per unit (p.u.). Similarly, the  $MAL$  is also expressed in p.u. The modified load is determined by adding the  $MAL$  with the base load as per the Eqs. (1) and (4) and the power factor is considered as 0.9. The value of base load,  $MAL$  and modified load of 33-bus system and 69-bus system are given in Tables 1 and 2, respectively. High value of  $MAL$  signifies that more extra load can be connected to the node without violating the practical security limits.

This signifies a greater number of EVs can be connected with the nodes having higher  $MAL$  Values. Considering this philosophy and based on the higher value of  $MAL$ , 8 EVCS at node 2, 3, 19, 20, 21, 22, 23, and 24 are chosen for 33-bus RDS. From the results of higher value of  $MAL$  and the single line diagram of 33-bus RDS, it can be concluded that the buses which are nearer to the generator have the capability to take more extra load without violating the voltage security limits. Similar kind of results are obtained for 69-bus RDS also.  $MAL$  is determined for all buses of 69-bus



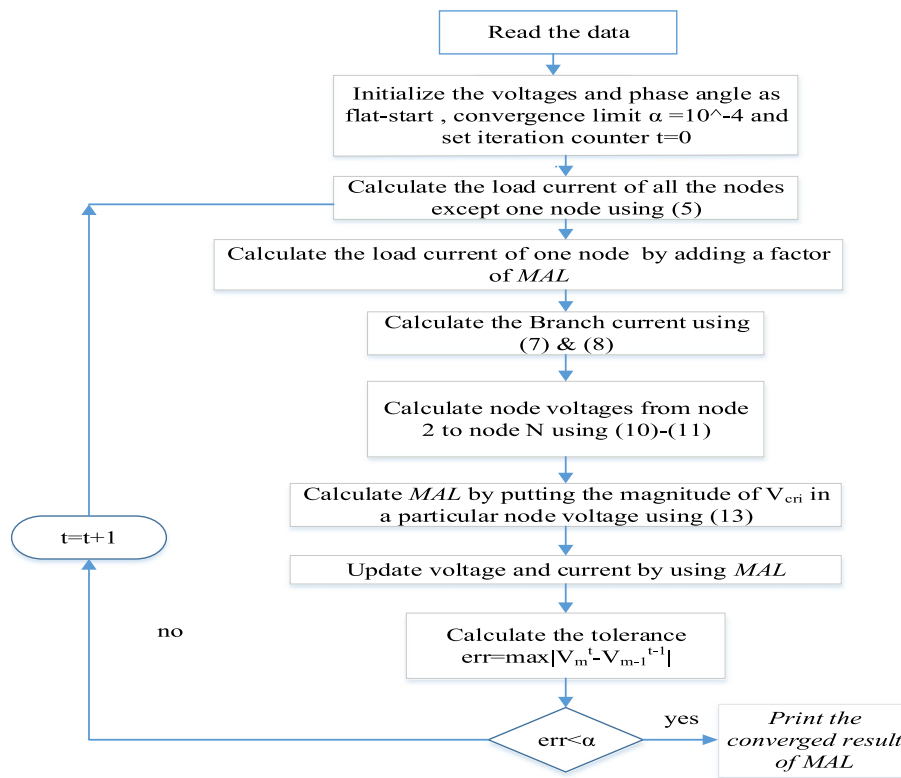


Fig. 2 Flowchart of MFBS algorithm

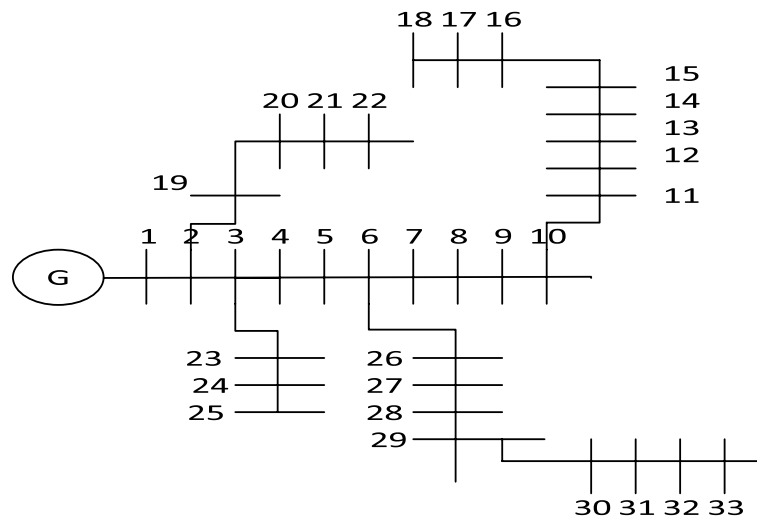
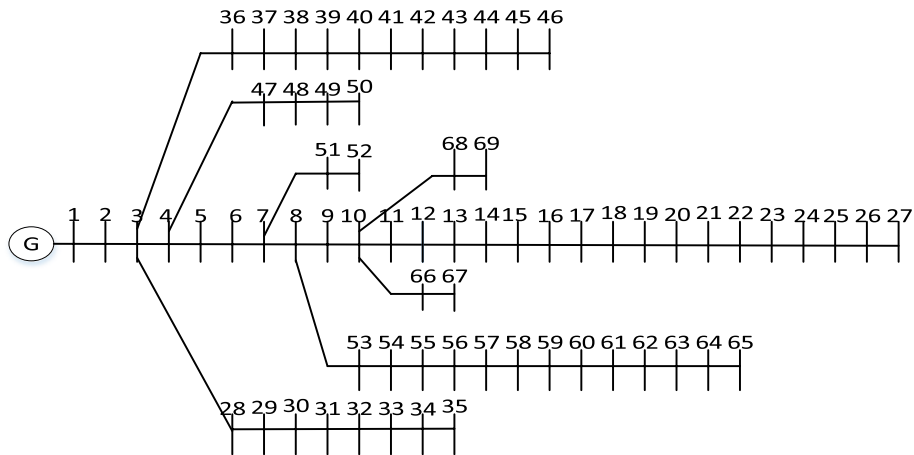


Fig. 3 Single line diagram of 33-bus RDS

RDS and based on the higher value of *MAL*, 8 nodes are identified. Accordingly, 8 EVCSs are selected for 69-bus RDS at node 6, 8, 66, 12, 68, 13, 14, and 16.

After application of *MAL*, the impact of the network should be checked. When *MAL* is applied on node 2, the modified voltage (MV) of 33-bus RDS is given in



**Fig. 4** Single line diagram of 69-bus RDS

**Table 1** Base load, maximum additional load, and modified load of 33-bus system

Node no	Base P(p.u.)	MAL(p.u.)	Modified P(p.u.)	Base Q(p.u.)	Modified Q(p.u.)
2	0.001	0.0477	0.0487	0.0006	0.02370111
19	0.0009	0.0473	0.0482	0.0004	0.02330739
20	0.0009	0.0438	0.0447	0.0004	0.02161234
21	0.0009	0.0428	0.0437	0.0004	0.02112804
22	0.0009	0.0411	0.0420	0.0004	0.02030473
3	0.0009	0.0074	0.0083	0.0004	0.00398382
23	0.0009	0.0073	0.0082	0.0005	0.00403539
24	0.0042	0.0072	0.0114	0.0020	0.00548696

**Table 2** Base load, maximum additional load, and modified load of 69-bus system

Node no	Base P(p.u.)	MAL(p.u.)	Modified P(p.u.)	Base Q(p.u.)	Modified Q(p.u.)
6	0.000026	0.0261	0.026126	0.000022	0.01265962
8	0.000750	0.0118	0.012550	0.000540	0.00625356
66	0.000180	0.0109	0.011080	0.000130	0.00540778
12	0.001400	0.0108	0.012200	0.001000	0.00622936
68	0.000280	0.0107	0.010980	0.000200	0.00538094
13	0.000080	0.0106	0.010680	0.000055	0.00518752
14	0.000080	0.0105	0.010580	0.000055	0.00513910
16	0.000455	0.0103	0.010755	0.000300	0.00528726

Table 3. The graphical representation of voltages at base load and MAL for 33-bus RDS is also shown in Fig. 5. From the Table 3 and Fig. 5, it is noticed that the voltage magnitudes are reduced after applying the MAL. It is also observed that all the system voltages are above the critical voltage ( $V_{cri}$ ), i.e., 0.9 p.u. after applying MAL at node 2 in the 33-bus system.

**Table 3** Voltage magnitude at base load and MFBS with MAL at node 2 for 33-bus system

Node no	Voltage at base load	Voltage after applying MAL at node 2	Node no	Voltage at base load	Voltage after applying MAL at node 2	Node no	Voltage at base load	Voltage after applying MAL at node 2
1	1	1	12	0.9177	0.9139	23	0.9793	0.9758
2	0.997	0.9936	13	0.9116	0.9077	24	0.9726	0.9691
3	0.9829	0.9794	14	0.9093	0.9054	25	0.9693	0.9658
4	0.9754	0.9718	15	0.9078	0.904	26	0.9476	0.9439
5	0.968	0.9644	16	0.9065	0.9026	27	0.945	0.9413
6	0.9495	0.9458	17	0.9044	0.9006	28	0.9335	0.9298
7	0.946	0.9423	18	0.9038	0.9	29	0.9253	0.9216
8	0.9323	0.9286	19	0.9965	0.993	30	0.9218	0.918
9	0.926	0.9222	20	0.9929	0.9894	31	0.9176	0.9138
10	0.9201	0.9163	21	0.9922	0.9887	32	0.9167	0.9129
11	0.9192	0.9155	22	0.9916	0.9881	33	0.9164	0.9126

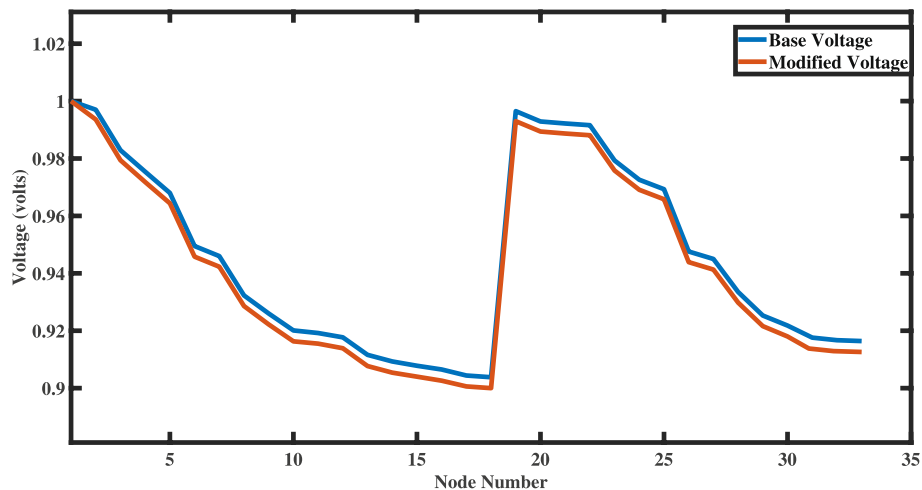


**Fig. 5** Graphical representation of the voltage of 33-bus RDS with and without MAL

For 33-bus RDS the critical voltage is obtained at node 18 after applying MAL on node 2. One important point is noticed that though MAL is applied on node 2 of 33-bus RDS, the critical voltage is obtained in the other node, i.e., node 18.

The voltage magnitudes of 69-bus RDS is given in Table 4 for base load and MAL. At node 6 MAL is applied for 69-bus RDS. The graphical representation of the voltages is shown in Fig. 6. In this test system, the voltage magnitudes are also reduced, and no bus voltage is below the critical voltage like 33-bus RDS. From the Table 4 and Fig. 6 it is noticed that the critical voltage is found at node 65 of 69-bus RDS. In this test system it is also observed that the critical voltage is obtained at node 65 which is different from the node where MAL is applied.

The proposed MFBS load flow is basically developed to determine the optimum capacity of EVCS. Practically, it is noteworthy that the power ratings of the EVs are mentioned in kW. Based on their state of charge (SOC) and amount of time till their departure time, EVCS can fulfil the requirement of the EVs through parallel multi-port. From MAL

**Table 4** Voltage magnitude at base load and MFBS with MAL at node 6 for 69-bus system

Node no	Voltage at base load	Voltage after applying MAL at node 6	Node no	Voltage at base load	Voltage after applying MAL at Node 6	Node no	Voltage at base load	Voltage after applying MAL at node 6
1	1	1	24	0.9566	0.9479	47	0.9998	0.9997
2	1	0.9999	25	0.9564	0.9477	48	0.9985	0.9985
3	0.9999	0.9999	26	0.9564	0.9476	49	0.9947	0.9946
4	0.9998	0.9997	27	0.9563	0.9476	50	0.9942	0.9941
5	0.999	0.9983	28	0.9999	0.9999	51	0.9785	0.97
6	0.9901	0.9817	29	0.9999	0.9998	52	0.9785	0.97
7	0.9808	0.9723	30	0.9997	0.9997	53	0.9747	0.9661
8	0.9786	0.9701	31	0.9997	0.9997	54	0.9714	0.9628
9	0.9774	0.9689	32	0.9996	0.9996	55	0.9669	0.9583
10	0.9724	0.9639	33	0.9993	0.9993	56	0.9626	0.9539
11	0.9713	0.9628	34	0.999	0.999	57	0.9401	0.9312
12	0.9682	0.9596	35	0.9989	0.9989	58	0.929	0.92
13	0.9653	0.9566	36	0.9999	0.9999	59	0.9248	0.9157
14	0.9624	0.9537	37	0.9997	0.9997	60	0.9197	0.9106
15	0.9595	0.9508	38	0.9996	0.9996	61	0.9123	0.9031
16	0.959	0.9503	39	0.9995	0.9995	62	0.912	0.9029
17	0.9581	0.9494	40	0.9995	0.9995	63	0.9117	0.9025
18	0.9581	0.9494	41	0.9988	0.9988	64	0.9098	0.9005
19	0.9576	0.9489	42	0.9986	0.9985	65	0.9092	0.9
20	0.9573	0.9486	43	0.9985	0.9985	66	0.9713	0.9627
21	0.9568	0.9481	44	0.9985	0.9985	67	0.9713	0.9627
22	0.9568	0.9481	45	0.9984	0.9984	68	0.9679	0.9592
23	0.9568	0.948	46	0.9984	0.9984	69	0.9679	0.9592

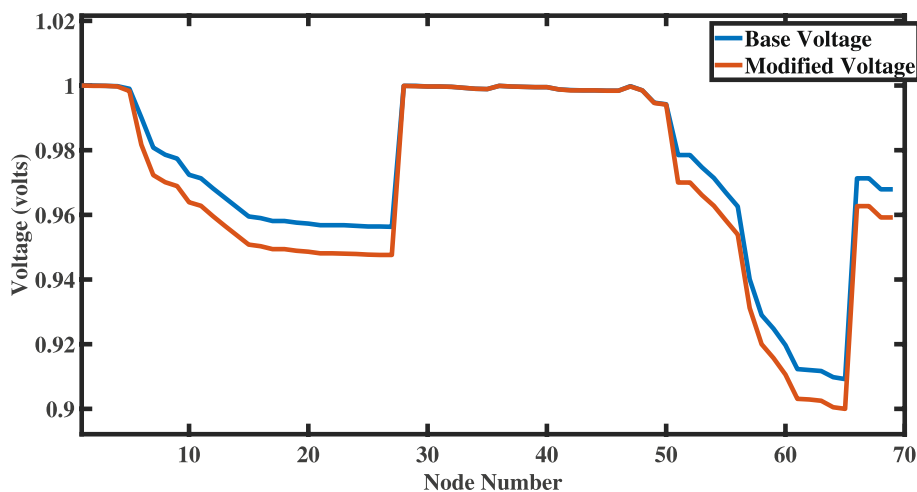


**Fig. 6** Graphical representation of the voltage of 69-bus RDS with and without MAL

information, the maximum rating of EVCS for a node can be obtained easily. Maximum ratings of EVCSs are given in Tables 5 and 6 for 33-bus and 69-bus RDS, respectively.

An EV’s charging priority changes dynamically while it is in the charging park, so it may leap from one priority level to a higher one just before leaving. In [32], total 5

**Table 5** Maximum ratings of EVCSs for 33-bus system

Node no	Base P(kW)	MAL (kW)	Modified P(kW)	Base Q(kVAR)	Modified Q(kVAR)
2	100	4770	4870	60	2370.111
19	90	4730	4820	40	2330.739
20	90	4380	4470	40	2161.234
21	90	4280	4370	40	2112.804
22	90	4110	4200	40	2030.473
3	90	740	830	40	398.382
23	90	730	820	50	403.539
24	420	720	1140	200	548.696

**Table 6** Actual loading Information of 69-bus system

Node no	Base P(kW)	MAL (kW)	Modified P(kW)	Base Q(kVAR)	Modified Q(kVAR)
6	2.6	2610	2612.6	2.2	1265.962
8	75	1180	1255	54	625.356
66	18	1090	1108	13	540.778
12	140	1080	1220	104	622.936
68	28	1070	1098	20	538.094
13	8	1060	1068	5.5	518.752
14	8	1050	1058	5.5	513.91
16	45.5	1030	1075.5	30	528.726

different kind of charging levels are given. When EV is linked to the parking station, EVs in levels 1, 2, and 3 can only be charged because they consume a lot of energy or because their SOC is low, below 10%. Based on the literature [32] survey and EV battery charging limit, the average power requirements of any EV are 20 kW. This data is used to compute the number of electric vehicles that can be charged at a time. The number of EVs is calculated as follows:

$$N_{EV} = \left( \frac{MAL_{kW}}{20} \right), N_{EV} \in \text{integer} \quad (16)$$

Here,  $MAL_{kW}$  is the permissible extra load in kW,  $N_{EV}$  is the number of EVs. In Eq. (16), 20 is divided because the average power requirement of EV is considered as 20 kW as per the literature [32].

Number of EV can be charged at a time is shown in Table 7 for 33-bus system and Table 8 for 69-bus system. From the tables, it can be concluded that the sufficient number of EVs can be charged in parallel mode at a time. It is also observed that for 33-bus RDS more number of EVs can be utilised for the charging purpose compared to the 69-bus RDS.

### Overall discussion

After calculating  $MAL$  for the various nodes of 33-bus RDS, nodes having higher  $MAL$  are decided as the optimal location of the EVCS. It has been seen that the voltage of the EVCS-connected node, in addition to the voltages of the other nodes, is higher than the critical voltage limit, which is 0.9 p.u. It has been determined that the average loadability

**Table 7** No. of EV to be charged for 33-bus RDS

Node no	MAL (kW)	No. of EVs
2	4770	238
19	4730	236
20	4380	219
21	4280	214
22	4110	205
3	740	37
23	730	36
24	720	36

**Table 8** No. of EV to be charged for 69-bus RDS

Node no	MAL (kW)	No. of EVs
6	2610	130
8	1180	59
66	1090	54
12	1080	54
68	1070	53
13	1060	53
14	1050	52
16	1030	51

limit of each EVCS at 33-bus RDS is 3058 kW while the total capacity of EVCS at 33-bus RDS is 24,464 kW. Moreover, due to the lesser branches of the 33-bus RDS, lesser amount losses are associated with 33 bus RDS. Hence, the loadability limit of the nodes of the 33-bus RDS is higher with respect to the 69 bus RDS. It is observed that the maximum allowable load for the node 2 of the EVCS is 4776 kW which is higher than the *MAL* value of node 2 of RDS. Again, the voltage at node 2 changes from 0.9970 p.u. to 0.9936 p.u. when it is loaded to its maximum permissible level of 4776 kW. As a result, there is not a significant amount of voltage variation. The similar kind of observation is evaluated for the nodes 19, 20, 21, 22, 3, 23, and 24. Based on the obtained *MAL*, it can be seen that the EVCSs of 33 bus have the higher potential to charge the EV in quantity. For 33 Bus RDS, a total number of 1216 EVs can be charged on average, whereas for 69 Bus RDS, it is 504.

#### Discussion related to 69-bus RDS

The modified proposed method is applied on a large system, specifically a 69-bus RDS, to gain a better understanding of its capabilities. After calculating *MAL* for the various nodes of the 69-bus RDS, the optimal location of the EVCS is determined to be at the node with the highest value of *MAL* connected to it. In the case of 69-bus RDS, the EVCS connected node and other node's voltages exceed the critical voltage limit of 0.9 p.u. When compared to the RDS for 33-bus, the conventional non-elastic load that is already applied to the nodes of 69-bus is significantly higher. Furthermore, the power losses associated with 69-bus RDS are little higher than those associated with 33-bus

RDS because of the increased number of branches that are associated with 69-bus RDS. The EVCS at node 6 has a maximum load capacity of 2610 kW, making it one of the best possible locations for the system's various nodes. When it is loaded to its maximum allowable level of 2610 kW, the voltage at node 6 changes from 0.9901 p.u. to 0.9817 p.u. This represents a change of 0.194 V. Similar kind of observations are also assessed for the case of other EVCS connected nodes. Hence, the capacity of the EVCS is high for 33 bus RDS as compared to 69-bus RDS. It also has been determined that the average capacity of each EVCS on 69 buses is 1272 kW, which is lower when compared to the capacity of each EVCS on 33 buses, which is 3058 kW. When compared to 33-bus RDS, 69-bus RDS has a lower maximum loadability limit, which means that a lesser number of electric vehicle batteries can be connected to it in order to be charged. According to the *MAL* that is obtained, the EVCSs that are installed in different buses of 69-bus RDS, have the potential to charge a total of 504 electric vehicle batteries on average.

## Conclusions

In this paper, a modified FBS method is developed to find the maximum permissible load for each node of a RDS. The proposed method is validated on 33-bus and 69-bus RDS to determine the optimal location of EVCS. It is observed that all the node voltages of these RDS, are above the lower range of voltage security limit for safe and secure power system operation, after installing the EVCS. The existing conventional non-elastic load for the nodes of 69-bus is higher as compare to the 33-bus RDS. Moreover, power losses for the case of 69-bus RDS are greater than those for 33-bus RDS as a direct consequence of the increased number of branches associated with 69-bus RDS. Hence, the capacity of the EVCS is higher at 33-bus RDS. It is obtained that the average loadability limit of each EVCS at 33-bus and 69-bus RDS are 3058 kW and 1272 kW respectively, whereas the total capacity of EVCS at 33-bus and 69-bus RDS are 24,464 kW and 10,176 kW. As the maximum loadability limit of 33-bus is high, hence more number of EV batteries can be connected for charging in case of 33-bus RDS compared to 69-bus RDS. On an average total 1216 and 504 EV batteries may be charged from the EVCSs of 33-bus and 69-bus RDS. Hence, it can be said that the proposed algorithm is efficient enough for maintaining the node voltages during EV charging process for both higher and lower bus RDS.

## Abbreviations

EVCS	Electric vehicle charging station
<i>MAL</i>	Maximum additional load
RDS	Radial distribution system
FBS	Forward backward sweep
SOC	State of charge
$P_{mod}$	Modified active power
$Q_{mod}$	Modified reactive power
$P_{Li}$	Real load power
$Q_{Li}$	Reactive load power
$I_i$	Load current
$I_m^{CP}$	Modified load current at <i>m</i> th node
$I_{ab}$	Current flowing through branch <i>a-b</i>
$I_{m-1,m}$	Current flowing through branch ( <i>m-1</i> )- <i>m</i>
$V_a$ & $V_b$	Voltage of node <i>a</i> and <i>b</i> respectively
$Z_{m-1,m}$	Impedance between node ( <i>m-1</i> ) & <i>m</i>
$Z_{ab}$	Impedance of branch <i>a-b</i>
$V_{cri}$	Magnitude of critical voltage
$V_m$	<i>m</i> Th node voltage

**Acknowledgements**

I would like to acknowledge NIT Durgapur for providing high-class internet and for giving access to download research papers for literature survey.

**Authors' contributions**

Roles for all authors are equal because everyone equally contributed to the research and article preparation. All authors read and approved the final manuscript.

**Funding**

The authors affirm that they were not provided with any financing.

**Availability of data and materials**

The entire modified method is applied in 33-bus and 69-bus radial distribution system. The data of these two systems are taken from reference [30, 31].

**Declarations****Competing interests**

The authors declare that they have no competing interests.

Received: 3 February 2023 Accepted: 20 April 2023

Published online: 10 May 2023

**References**

1. Tu JC, Yang C (2019) Key factors influencing consumers' purchase of electric vehicles. *Sustainability* 11(14):3863. <https://doi.org/10.3390/su11143863>
2. Ehsani M, Gao Y, Longo S, Ebrahimi KM (2018) Modern electric, hybrid electric, and fuel cell vehicles. CRC press. <https://doi.org/10.1201/9780429504884>
3. Ye Z, Gao Y, Yu N (2022) Learning to operate an electric vehicle charging station considering vehicle-grid integration. *IEEE Trans Smart Grid* 13(4):3038–3048. <https://doi.org/10.1109/TSG.2022.3165479>
4. Singh PP, Wen F, Palu I, Sachan S, Deb S (2022) Electric vehicles charging infrastructure demand and deployment: challenges and solutions. *Energies* 16(1):7. <https://doi.org/10.3390/en16010007>
5. Danese A, Torsæter BN, Sumper A, Garau M (2022) Planning of high-power charging stations for electric vehicles: a review. *Appl Sci* 12(7):3214. <https://doi.org/10.3390/app12073214>
6. Acharige S S, Haque M E, Arif M T, Hosseinzadeh N (2022) Review of electric vehicle charging technologies, configurations, and architectures. arXiv preprint [arXiv:2209.15242](https://arxiv.org/abs/2209.15242). <https://doi.org/10.48550/arXiv.2209.15242>
7. Johansson S, Persson J, Lazarou S, Theocharis A (2019) Investigation of the impact of large-scale integration of electric vehicles for a Swedish distribution network. *Energies* 12(24):4717. <https://doi.org/10.3390/en12244717>
8. Bedoud K, Merabet H, Bahi T (2022) Power control strategy of a photovoltaic system with battery storage system. *J Eng Appl Sci* 69(1):1–20. <https://doi.org/10.1186/s44147-022-00163-8>
9. Hameed F, Al Hosani M, Zeineldin HH (2017) A modified backward/forward sweep load flow method for islanded radial microgrids. *IEEE Trans Smart Grid* 10(1):910–918. <https://doi.org/10.1109/TSG.2017.2754551>
10. Gao B, Morison GK, Kundur P (1992) Voltage stability evaluation using modal analysis. *IEEE Trans Power Syst* 7(4):1529–1542
11. Zhang M, Li Y (2020) Multi-objective optimal reactive power dispatch of power systems by combining classification-based multi-objective evolutionary algorithm and integrated decision making. *IEEE Access* 8:38198–38209
12. Adebayo IG, Jimoh AA, Yusuff AA, Sun Y (2018) Analysis of voltage collapse in a power system using voltage stability indices. *JETP* 8(4)
13. Zheng C, Kezunovic, M (2010) Distribution system voltage stability analysis with wind farms integration. In: North American power symposium 2010, IEEE, pp 1–6
14. Dharmapala KD, Rajapakse A, Narendra K, Zhang Y (2020) Machine learning based real-time monitoring of long-term voltage stability using voltage stability indices. *IEEE Access* 8:222544–222555
15. Ismail B, Wahab NIA, Othman ML, Radzi MAM, Vijayakumar KN, Rahmat MK, Naain MNM (2022) New line voltage stability index (BVSI) for voltage stability assessment in power system: the comparative studies. *IEEE Access* 10:103906–103931
16. Song Y, Hill DJ, Liu T (2018) Static voltage stability analysis of distribution systems based on network-load admittance ratio. *IEEE Trans Power Syst* 34(3):2270–2280
17. Alshareef A, Shah R, Mithulananthan N, Alzahrani S (2021) A new global index for short term voltage stability assessment. *IEEE Access* 9:36114–36124
18. Razavi SE, Rahimi E, Javadi MS, Nezhad AE, Lotfi M, Shafie-khah M, Catalão JP (2019) Impact of distributed generation on protection and voltage regulation of distribution systems: a review. *Renew Sustain Energy Rev* 105:157–167. <https://doi.org/10.1016/j.rser.2019.01.050>
19. Dolatabadi SH, Ghorbanian M, Siano P, Hatzigiorgiuri ND (2020) An enhanced IEEE 33 bus benchmark test system for distribution system studies. *IEEE Trans Power Syst* 36(3):2565–2572. <https://doi.org/10.1109/TPWRS.2020.3038030>
20. Xu B, Zhang G, Li K, Li B, Chi H, Yao Y, Fan Z (2022) Reactive power optimization of a distribution network with high-penetration of wind and solar renewable energy and electric vehicles. *Prot Control Mod Power Syst* 7(1):51. <https://doi.org/10.1186/s41601-022-00271-w>



21. Shirmohammadi D, Hong HW, Semlyen A, Luo GX (1988) A compensation-based power flow method for weakly meshed distribution and transmission networks. *IEEE Trans Power Syst* 3(2):753–762. <https://doi.org/10.1109/59.192932>
22. Das D, Nagi HS, Kothari DP (1994) Novel method for solving radial distribution networks. *IEE Proc Gener Transm Distrib* 141(4):291–298
23. Baran ME, Wu FF (1989) Optimal capacitor placement on radial distribution systems. *IEEE Trans Power Deliv* 4(1):725–734. <https://doi.org/10.1109/61.19265>
24. Baran M, Wu FF (1989) Optimal sizing of capacitors placed on a radial distribution system. *IEEE Trans Power Deliv* 4(1):735–743. <https://doi.org/10.1109/61.19266>
25. Reddy V V K, Sydulu M (2007) 2Index and GA based optimal location and sizing of distribution system capacitors. In: 2007 IEEE Power Engineering Society General Meeting, IEEE, pp 1–4. <https://doi.org/10.1109/PES.2007.385547>
26. Ghosh S, Das D (1999) Method for load flow solution of radial distribution networks. *IEE Proc Gener Transm Distrib* 146(6):641–648
27. Thukaram DHMW, Banda HW, Jerome J (1999) A robust three phase power flow algorithm for radial distribution systems. *Electr Power Syst Res* 50(3):227–236. [https://doi.org/10.1016/S0378-7796\(98\)00150-3](https://doi.org/10.1016/S0378-7796(98)00150-3)
28. Cheng CS, Shirmohammadi D (1995) A three-phase power flow method for real-time distribution system analysis. *IEEE Trans Power Syst* 10(2):671–679. <https://doi.org/10.1109/59.387902>
29. Kersting WH (1984) A method to teach the design and operation of a distribution system. *IEEE Trans Power Appar Syst* 7:1945–1952. <https://doi.org/10.1109/TPAS.1984.318663>
30. University of Washington. Power systems test case archive. Accessed 12 June 2017.
31. Goswami SK, Basu SK (1992) A new algorithm for the reconfiguration of distribution feeders for loss minimization. *IEEE Trans Power Deliv* 7(3):1484–1491. <https://doi.org/10.1109/61.141868>
32. Mohamed A, Salehi V, Ma T, Mohammed O (2013) Real-time energy management algorithm for plug-in hybrid electric vehicle charging parks involving sustainable energy. *IEEE Trans Sustain Energy* 5(2):577–586. <https://doi.org/10.1109/TSTE.2013.2278544>

### Publisher's Note

Springer Nature remains neutral with regard to jurisdictional claims in published maps and institutional affiliations.

**Submit your manuscript to a SpringerOpen<sup>®</sup> journal and benefit from:**

- ▶ Convenient online submission
- ▶ Rigorous peer review
- ▶ Open access: articles freely available online
- ▶ High visibility within the field
- ▶ Retaining the copyright to your article

---

Submit your next manuscript at ▶ [springeropen.com](https://www.springeropen.com)

---